Brain Multiphysics 2 (2021) 100024

Contents lists available at ScienceDirect

Brain Multiphysics

journal homepage: www.elsevier.com/locate/brain

A quantitative relationship between rotational head kinematics and brain tissue strain from a 2-D parametric finite element analysis

Rika Wright Carlsen[a,*], Alice Lux Fawzi[b], Yang Wan[b], Haneesh Kesari[b], Christian Franck[c]

[a] Department of Engineering, Robert Morris University, Moon Township, PA 15108, USA
[b] School of Engineering, Brown University, Providence, RI 02912, USA
[c] Department of Mechanical Engineering, University of Wisconsin-Madison, Madison, WI 53706, USA

ARTICLE INFO

Keywords:
Traumatic brain injury
Finite element modeling
Head kinematics
Parametric study
Brain strain

ABSTRACT

Given the complex nature of traumatic brain injury (TBI), assessment of injury risk directly from kinematic measures of head motion remains a challenge. Despite this challenge, kinematic-based measures of injury continue to be widely used to guide the design of protective equipment. In an effort to provide more insight into the relationship between rotational head kinematics and injury risk, we have conducted a large scale parametric finite element analysis (FEA) to investigate the role of angular acceleration, angular velocity, and angular jerk on the brain tissue strains and strain rates. The peak strains and strain rates resulting from rotational head accelerations were obtained for peak angular accelerations ranging from 0.5 - 25 krad/s^2 and peak angular velocities ranging from 10 - 100 rad/s. The results of this study show that both angular acceleration and angular velocity have a significant effect on the peak tissue strains and strain rates, reinforcing the importance of accounting for both of these kinematic measures when evaluating injury risk. For a given magnitude of peak angular acceleration and angular velocity, increases in angular jerk are shown to have minimal effect on the peak tissue strains but can lead to an increase in the peak tissue strain rates. This advancement in our understanding of the relationship between angular head kinematics, tissue strain, and tissue strain rate is an important step toward developing improved kinematic-based measures of injury.

Statement of Significance

To reduce the risk of traumatic brain injury, we must first fully understand the relationship between impact-induced head motions and the brain deformation response. Large deformations of the brain have been shown to cause damage to neural cells and can result in long-term neurocognitive deficits. This study investigates the role of angular acceleration, angular velocity, and angular jerk on the tissue strains and strain rates that develop in the brain. By providing further insight into how each of these kinematic parameters affect the brain deformation response, we can begin to identify the types of head motions that are the most injurious and develop new targeted approaches to reduce the risk of injury.

1. Introduction

Traumatic brain injury (TBI) is a debilitating condition that can lead to long-term cognitive and physical impairments. It can be caused by sudden inertial loading of the head, which can result from blunt trauma or from exposure to blasts. There has been a focused effort to develop new injury prevention protocols and protective equipment for TBI to reduce the risk and severity of injury. Kinematic-based tolerance thresholds for injury are often used to guide the design and to assess the effectiveness of these measures [1]. Although a large number of head kinematic injury criteria and tolerance thresholds have been proposed for TBI, given the complex nature of brain injury, there is still no consensus on the best measure to use when developing new injury mitigation strategies.

Further insight into the relationship between head kinematics and brain deformation is needed to guide the development of new injury prevention measures. Rotational accelerations and velocities are of particular concern as key contributors to injury [2]. In this study, we investigate the role of rotational head acceleration, velocity, and jerk on the tissue strains and strain rates that develop within the brain through a large scale parametric analysis. Both strain and strain rate have been shown to play an important role in axonal injury, which is one of the

* Corresponding author.

https://doi.org/10.1016/j.brain.2021.100024
Received 13 October 2020; Received in revised form 13 March 2021; Accepted 14 March 2021

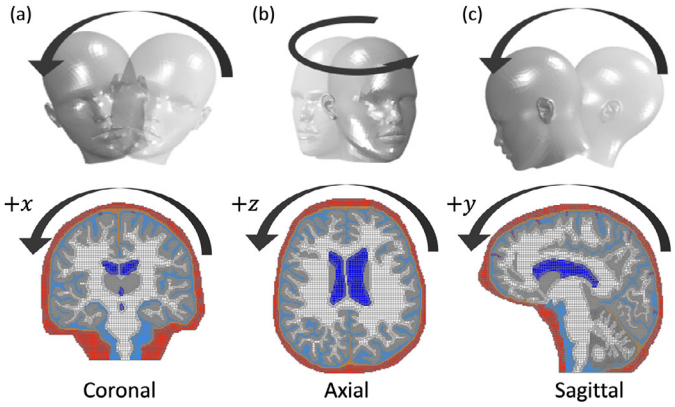

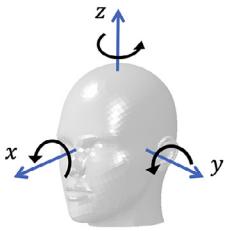

Fig. 1. The effect of head rotation on the brain tissue deformation was assessed using 2-D finite element head models representing the (a) coronal, (b) axial, and (c) sagittal planes. Angular accelerations were applied in the direction shown about the head center of mass (i.e., in the positive x, y, and z rotation directions). The finite element models included the skull (red), cerebral spinal fluid (light blue), ventricles (dark blue), falx cerebri (orange), tentorium cerebellum (orange), bridging veins (purple), white matter (white), and gray matter (gray).

main pathological features of TBI [3–5]. Mechanical stretch of neuronal axons at high strain rates has been shown to cause rupture of cytoskeletal structures, mechanoporation, and initiate biochemical signaling cascades that can ultimately result in cell death [5–7]. Proposed strain thresholds for neural injury typically range between 10% and 25% [3,4,7–12]. The effect of strain rate on injury has not been as extensively studied; however, there is evidence that an increase in strain rate can lead to an increased probability of injury [3,7,10,13–17]. In vitro studies have shown that neurons subjected to high rates of loading ($> 10\ s^{-1}$) have an increased likelihood of cell death compared to neurons loaded at quasi-static rates [7,16]. Animal studies have also found a strong correlation between axonal injury and axonal deformation measures [3,17]. An optimal axonal strain rate injury threshold range of 40 - 90 s^{-1} has recently been defined using a porcine model of TBI [17]. Although more work is needed to define appropriate tissue-based tolerance thresholds that account for both of these deformation measures, there is a general consensus that interventions that reduce the tissue strains and strain rates in the brain will lead to a lower risk of injury.

Given the importance of mechanical strain and strain rate in injury development, there is a critical need to map head kinematics to tissue-based deformation measures to assess injury risk. Since the tissue strains within the brain have been shown to be primarily caused by rotational head motions [2,18], it is especially important to account for the effect of angular acceleration, angular velocity, and angular jerk on the brain deformation response. One of the most common approaches for relating strains and strain rates within the brain to head kinematics has been through the use of finite element (FE) head models. FE head models have been applied to reconstruct real-world head impact events and to correlate brain deformation measures with injury diagnosis and structural changes in the brain following a head impact [4,12,19–24]. Through this approach, both kinematic and tissue deformation-based injury metrics have been derived [9,11,25–27]. While most of these studies focus on the ability of FE models to predict the presence of injury, recent studies have also investigated the capability of FE models to predict the location of axonal injury in the brain [3,17]. A study by Hajiaghamemar and Margulies has shown that the sites of axonal injury in pigs subjected to rapid head rotation could be predicted within 2.5 mm using an FE head model [17]. These studies demonstrate the promising potential of FE models to predict the severity and distribution of injury in the brain.

While finite element head models allow us to study the brain deformation response, these simulations are computationally expensive, often taking several hours or tens of hours to run depending on the spatial resolution and numerical methods that are implemented [28–30]. Therefore, there is also a need to develop simple models through either physics-based or empirical approaches that allow for the rapid assessment of the peak tissue strains and strain rates, which would save considerable time in the design process of new protective equipment and in the assessment of new injury mitigation strategies. Several studies have applied a physics-based approach to study the relationship between rotational head kinematics and brain deformation and showed good agreement between the peak strains predicted with a mass-spring-damper mechanical system and that predicted with a finite element head model [31–34]. These mechanical models were validated against finite element predictions for a subset of impact conditions. In this study, we perform a large scale parametric analysis to investigate the relationship between head kinematics and tissue strain and strain rate. An idealized acceleration loading profile is applied to biofidelic 2-D finite element head models, simulating angular rotations about the three main anatomical axes. The results of this study provide a physics-based perspective on the relationship between angular kinematics and brain deformation. The insight gained this study can be applied to develop new approaches for rapidly estimating the brain deformation response and assessing injury risk.

The rest of this paper is organized as follows. The finite element head models and the design of the parametric study are presented in Section 2. In the parametric study, the peak angular acceleration and peak angular velocity of the head are varied to cover the range of accelerations and velocities typically encountered in common head impact scenarios (e.g., sports, falls, etc.). We also explore the effect of angular jerk on the brain deformation response, which has not been as extensively studied as other kinematic measures. Results from the parametric analysis are presented in Section 3. Finally, the significance of the results are discussed in Section 4, highlighting the important role of the angular kinematic parameters on the brain deformation response.

2. Methods

2.1. Finite Element Head Models

The parametric study was conducted using two-dimensional human head finite element (FE) models representing the coronal, axial, and sagittal planes as shown in Figure 1. The 2-D FE models are described briefly here, but further details about the model development and validation can be found in Wright et al. [35]. The FE models were generated from T1-weighted magnetic resonance images (MRI) and diffusion tensor images (DTI) of a single normal adult subject and include the major anatomical structures, such as the skull, dura mater (including falx cerebri and tentorium cerebellum), bridging veins, cerebral spinal fluid, ventricles, white matter, and gray matter. Each finite element model consists of about 10,000 elements, including 4-node bilinear, reduced integration with hourglass control and 3-node linear elements. The element size (1 to 2 mm) is comparable to the spatial resolution of the imaging data. The brain tissue was modeled using an anisotropic hyperviscoelastic strain energy function where the local fiber alignment direction and degree of fiber dispersion were obtained from DTI data. A Mie-Gruneisen equation of state was applied to define the hydrostatic behavior of the fluid regions, and the deviatoric behavior was defined through a shear viscosity. The skull was treated as a rigid solid. A table of the material properties can be found in the Supplementary Materials.

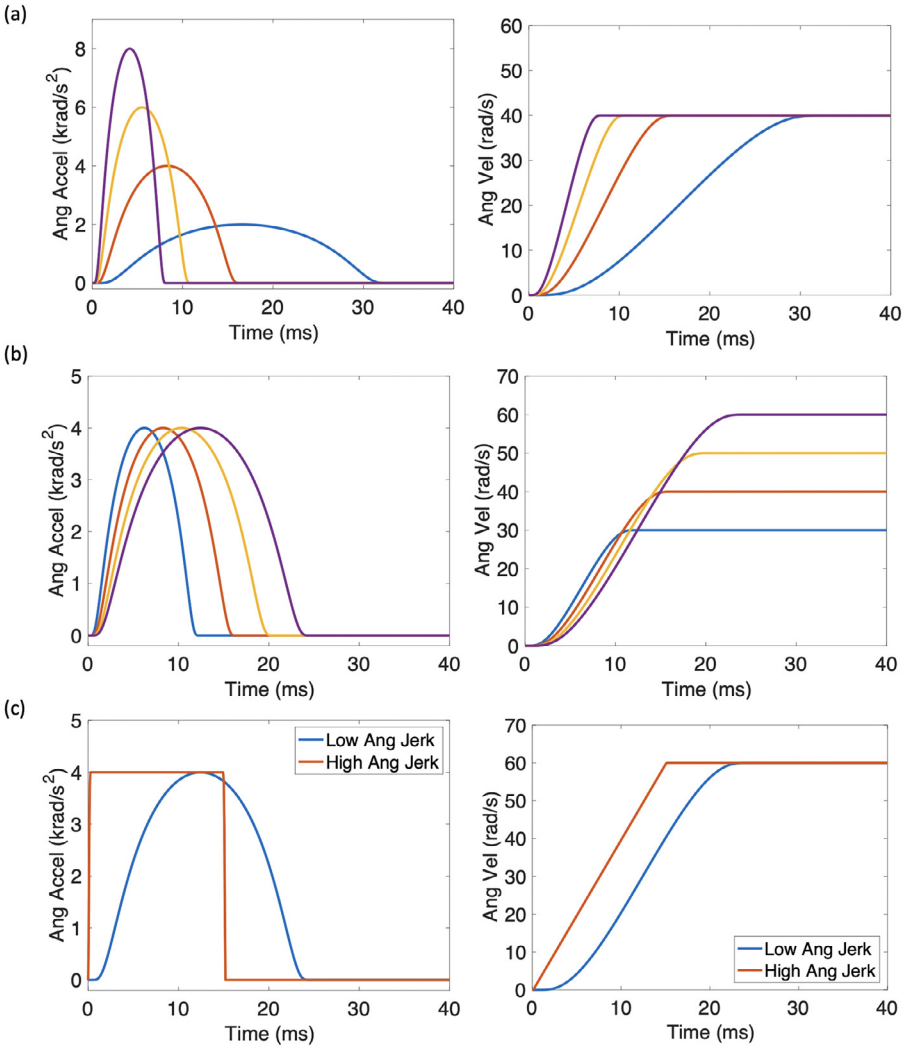

Fig. 2. Representative angular acceleration (left) and corresponding angular velocity (right) time histories are shown. The angular acceleration profiles were applied to the finite element models in the parametric study. In (a), the peak angular acceleration is varied while holding the peak angular velocity constant. In (b), the peak angular velocity is varied while holding the peak angular acceleration constant. In (c), the angular jerk is varied while holding the peak angular acceleration and peak angular velocity constant.

The finite element head models have previously been validated against several experimental datasets, including both low and high rate head impact data [35]. The intracranial pressure response was compared to pressure measurements from a cadaveric head impact test by Nahum et al. [36], and the finite element models were shown to adequately capture the pressure time history [35]. The deviatoric response of the brain tissue at low strain rates was validated against in vivo strain measurements from tagged magnetic resonance imaging (tagged MRI) of human volunteers subjected to mild angular head accelerations [37]. The area fraction of the brain exceeding a shear strain threshold of 2%, 4%, and 6% was quantified during the loading history. Good agreement was found between the experimental and model-predicted results [35]. A CORA analysis [38] was performed with scores ranging from 0.520 to 0.679, corresponding to a "Fair" to "Good" biofidelity rating. We have also extended our analysis to include high-rate cadaveric head impact test data from Hardy et al. [39]. In these experimental tests, clusters of neutral density targets (NDT) implanted in the brain were tracked using bi-plane high-speed X-ray, and the tissue strains were computed from the displacement history of the targets. The experimental strain results from these head impact tests were recently reanalyzed by Zhou et al. [40], and this updated strain-time history data was compared to our model predictions. An acceptable level of agreement was found between the model predictions and the experimental results. The CORA scores ranged from 0.456 to 0.534, corresponding to a "Fair" biofidelity rating. More details about the validation studies are included in the Supplementary Materials.

2.2. Loading Condition

A series of angular acceleration loading profiles were applied to the FE head models to study the relationship between rotational head kinematics and brain tissue deformation. A continuously differentiable bump function was used to define the pulse shape of the acceleration loading profile as follows

$$\alpha(t) = \begin{cases} (\alpha_{max}) \exp\left(1 - \frac{1}{1-\left(\frac{2t}{\Delta t}-1\right)^2}\right) & 0 \le t \le \Delta t \\ 0 & \text{otherwise} \end{cases} \quad (1)$$

where $\alpha(t)$ is the angular acceleration, t is time, Δt is the pulse duration, and α_{max} is the peak angular acceleration magnitude. The peak angular acceleration occurs at $t = \Delta t/2$. This function was integrated to obtain the angular velocity ω and differentiated with respect to time to obtain the angular jerk ζ.

Using this loading profile, the desired peak angular acceleration, peak angular velocity, and peak angular jerk were applied to the FE head models. Representative angular acceleration and velocity loading profiles are shown in Figure 2. To study the effect of angular acceleration on the brain tissue response, the peak angular velocity was held constant while varying the peak angular acceleration (Figure 2a). The effect of angular velocity was studied by holding the peak angular acceleration constant while varying the peak angular velocity (Figure 2b). Finally, to study the effect of angular jerk, the angular jerk magnitude was varied

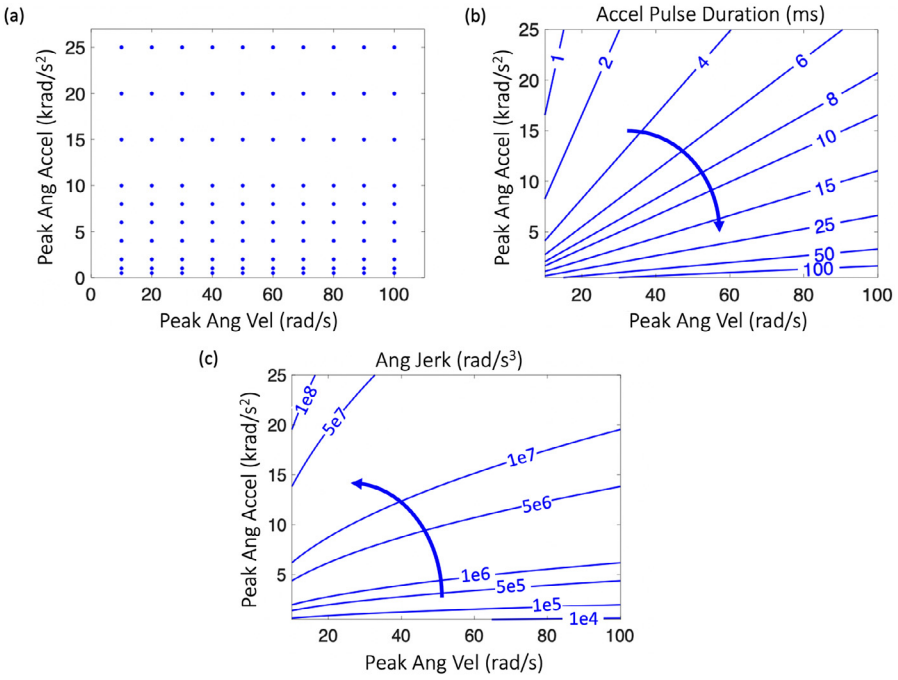

Fig. 3. (a) The parameter space that was covered in the parametric FE analysis is shown, where the circular blue markers represent the peak angular velocity and peak angular acceleration magnitudes that were simulated. Each data point represents a separate finite element simulation. The acceleration pulse duration and peak angular jerk are a function of the angular velocity and angular acceleration magnitudes as shown in the contour plots in (b) and (c), respectively. These results are shown for the low angular jerk case, and the arrows indicate the directions of increasing pulse duration or angular jerk.

while holding the peak angular acceleration and peak angular velocity constant (Figure 2c). The smooth bump function was applied to model the acceleration profile for the low jerk case (blue curve in Figure 2c). For the high jerk case, a bump function with a peak angular jerk that was 50 times larger than the low jerk profile was applied to generate the increasing and decreasing portions of the acceleration curve. After reaching the peak acceleration, the angular acceleration was held constant long enough to achieve the desired peak angular velocity as shown by the orange curve in Figure 2c.

The finite element analyses were conducted using an explicit time integration scheme in Abaqus/Explicit (Dassault Systémes), and a plane strain condition was assumed for the 2-D problem. To simulate rotational head motions, the angular acceleration loading profiles were applied directly to the rigid skull of the FE model, and the skull was rotated about the head center of mass. The skull was rotated in the directions shown in Figure 1. The simulation time was extended 20 ms beyond the end of the applied acceleration pulse for all simulations to give the shear waves enough time to propagate through the brain tissue to fully capture the strain response, which has been shown to be important in prior studies [41]. This is especially important for loading profiles with a short pulse duration (< 10 ms) since the tissue strains do not reach their maximum value before the end of the acceleration pulse. The acceleration magnitude was set to zero during the final 20 ms of the simulations. Each simulation utilized 12 cores on a high performance computer with an average wall clock time of about 0.6 minutes for 1 ms of simulation time.

2.3. Parametric Study

A large-scale parametric FE analysis was conducted to investigate the relationship between the applied inertial loads and the brain tissue response. The parametric study was designed to span a wide range of applied loading conditions representative of real-world head impact conditions, and the effect of both the peak angular acceleration and peak angular velocity on the maximum principal tissue strains and strain rates was analyzed. Figure 3a shows the parameter space. Each data point represents a single simulation that was conducted using the methods described in Section 2.2. The peak angular velocity was varied between 10 and 100 rad/s, and the peak angular acceleration was varied between 0.5 and 25 krad/s^2. The upper values of these kinematic parameters were chosen based on measured head impact events. Angular accelerations up to 25 krad/s^2 have been recorded in head impacts of mixed martial arts (MMA) fighters [42], and angular velocities up to 100 rad/s have been recorded in concussive sports impacts [34].

From the angular velocity and angular acceleration values, the acceleration pulse duration and peak angular jerk can be computed. Contour plots of the pulse duration and peak angular jerk are shown for the low angular jerk case in Figures 3b and 3 c, respectively. The pulse duration ranged from 0.7 ms to 331 ms for the low angular jerk case, and it ranged from 0.4 ms to 203 ms for the high angular jerk case. The peak angular jerk magnitude ranged from 6.5×10^3 rad/s^3 to 1.6×10^8 rad/s^3 for the low angular jerk case, with the angular jerk magnitudes being 50 times larger for the high angular jerk case. A total of one-hundred simulations were conducted to cover the parameter space. This parametric study was repeated for each finite element head model (coronal, axial, and sagittal) and for both the low angular jerk and high angular jerk acceleration loading profiles, resulting in a total of six-hundred simulations.

2.4. Analysis

The finite element analysis results were post-processed to obtain the maximum principal strains (MPS) and maximum principal strain rates (MPSR) within the brain tissue. At each time point of the simulation, the 95th percentile logarithmic MPS value was obtained for the brain (i.e., 95% of the brain tissue elements have a strain magnitude at or below this value). The 95th percentile value (instead of the 100th percentile value) is commonly used in finite element studies to limit the effect of numerical artifacts on the results [28]. The peak strain for a given simulation was defined as the maximum value of the 95th percentile MPS during the time history of the simulation. The peak strain rates were similarly obtained from the 95th percentile logarithmic MPSR values.

To analyze the effect of using an anisotropic definition of strain on the results, the maximum axonal strain (MAS) and maximum axonal strain rate (MASR) were also assessed in the white matter regions of the brain. Unlike the gray matter, which consist of neuronal cell bodies and is considered isotropic, the white matter consists of aligned axonal fibers and is considered to be anisotropic. Prior studies have proposed the use of an anisotropic measure of strain to evaluate the risk of axonal injury [22,24,43–47]. In this study, the axonal strain is defined as the loga-

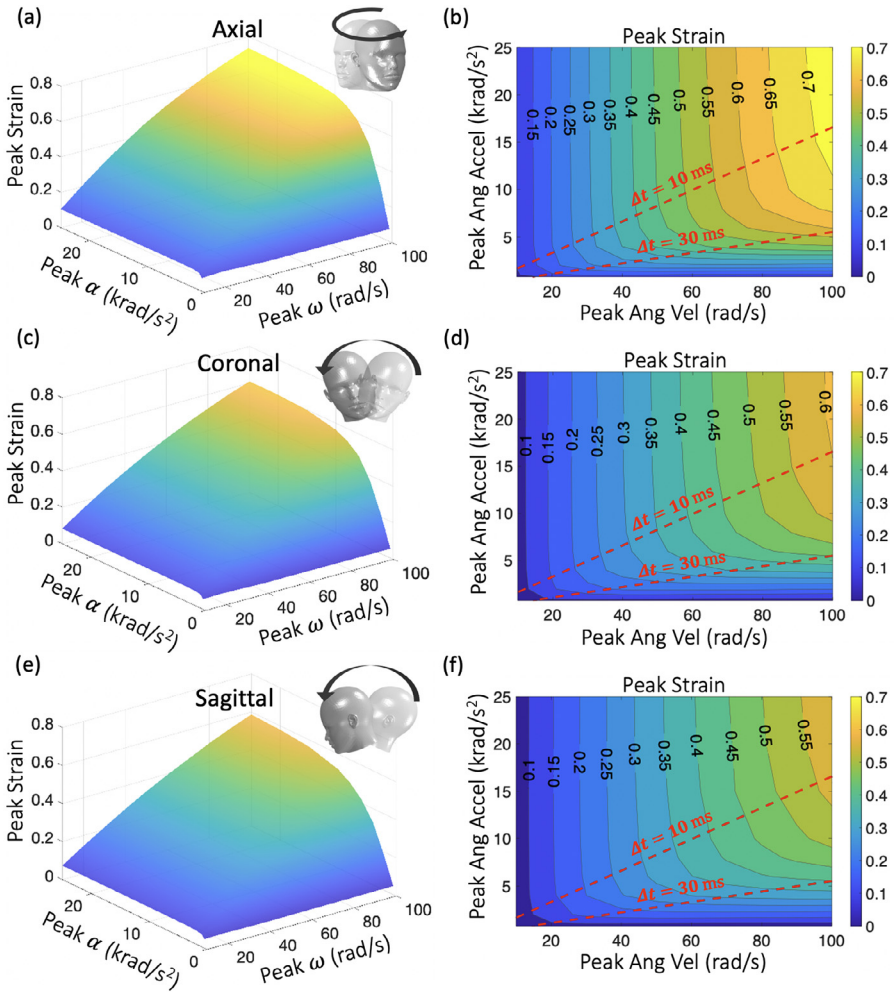

Fig. 4. The effect of angular velocity ω and angular acceleration α on the peak tissue strain is shown. In the left column, the peak tissue strain is plotted along the vertical axis in the 3-D surface plots, and the results are shown for the (a) axial, (c) coronal, and (e) sagittal models. In the right column, contour plots of the peak tissue strains are shown for the (b) axial, (d) coronal, and (f) sagittal models.

rithmic strain component resolved in the direction of fiber alignment. Likewise, the axonal strain rate is the logarithmic strain rate component resolved in the direction of fiber alignment. Since the FE head models are two-dimensional, the fiber alignment directions were obtained by projecting the 3-D fiber orientation vectors from diffusion tensor imaging onto the 2-D plane of the models. The fiber orientations were initially defined in the reference configuration and were allowed to rotate with the material as it deformed. The axonal strain was defined based on the direction of fiber alignment in the deformed configuration. The 95th percentile axonal strain (MAS) and 95th percentile axonal strain rate (MASR) were obtained within the white matter regions of the brain at each time point of the simulations. The peak values of MAS and MASR for a given simulation were defined as the maximum value of the 95th percentile MAS and the maximum value of 95th percentile MASR over the time history of the simulation.

Contour plots and 3-D surface plots relating the peak angular acceleration, peak angular velocity, and peak strains (or peak strain rates) were generated to investigate the effect of the applied loading conditions on the brain deformation response. Separate plots were generated for each rotation direction (axial, coronal, and sagittal). Normalized strain and strain rate distribution plots were also created to show the locations of the brain that experience the largest strain and strain rates over the time history of the simulations. In these plots, the peak value of the MPS from each brain tissue element was extracted over the course of each simulation. The MPS values were then normalized by the 95th percentile MPS for a given kinematic condition. Finally, cumulative strain maps and strain rate maps were created to identify those regions with strain and strain rate magnitudes above a given threshold. To generate the cumulative strain and strain rate maps, the 95th percentile MPS and MPSR were tracked for all brain tissue elements (white and gray matter) during the time history of the simulations. Any elements that exceeded a strain value of 15% or strain rate value of 40 s^{-1} at any time point of the simulation were identified and highlighted in the brain maps. These threshold values were chosen since they fall within the range of strain and strain rate injury tolerance thresholds that have been proposed for axonal injury [3,4,7–17]. The area fraction of the brain tissue that exceeds each of the threshold values was also computed. This area fraction metric is similar to the cumulative strain damage measure (CSDM) commonly used to assess brain injury in finite element studies of TBI [25], which is based on the total volume fraction of brain tissue that exceeds a given MPS threshold.

3. Results

3.1. Effect of Head Kinematics on Peak Strains

The peak tissue strains resulting from the parametric study are shown in Figure 4. These results were obtained by applying the low angular jerk acceleration loading profiles in the rotation directions shown. In the left column of the figure, three-dimensional surface plots of the peak strain are shown for head rotations about the axial, coronal, and sagittal planes. The peak strain values are plotted along the vertical axis, and the peak angular acceleration and peak angular velocity magnitudes are plotted along the horizontal axes. The 3-D surfaces were fitted to the peak strain values using piecewise linear interpolation. In the right column of Figure 4, the same peak strains from the surface plots are represented as contour plots. These results show that for the same applied loading conditions, axial rotations produced the largest brain tissue strains, followed by coronal rotations, and then sagittal rotations. The maximum percent difference in the peak strains between the axial

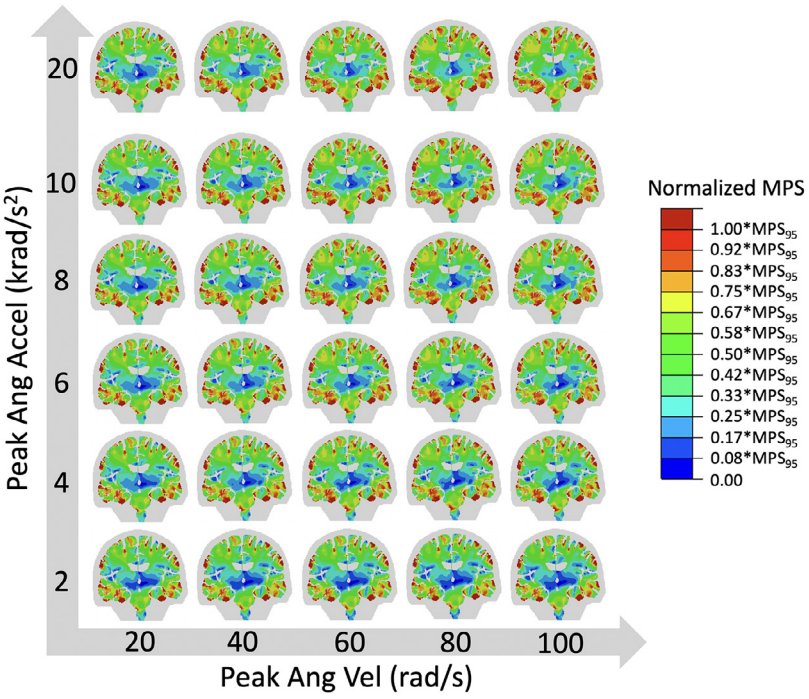

Fig. 5. The normalized maximum principal strain (MPS) distribution within the coronal plane is plotted for different applied magnitudes of angular acceleration and angular velocity. The strain distribution represents the peak MPS from each brain tissue element over the course of a simulation. The magnitude of the strains for each kinematic condition have been normalized by the 95th percentile strain value (MPS_{95}) for that kinematic condition, which can be obtained from Figure 4.

and coronal models was 34.7%, and the maximum percent difference between the coronal and sagittal models was 17.1%. Positive and negative rotation directions within a given plane did not have a significant effect on the peak strains. For example, the maximum percent difference in the peak strains for sagittal rotations in the positive and negative direction (as defined in Figure 1) was 3.1%, with an average percent difference of 0.9%.

The shape of the strain contours in Figure 4 provide insight into the relationship between tissue strain, angular acceleration, and angular velocity. The contours have a similar shape for all three head rotation directions. The strain contours tend to be vertical at larger acceleration magnitudes and horizontal at lower acceleration magnitudes with a transition zone occurring in-between. This general shape of the strain contours has also been observed in prior studies [3,31,48]. The transition zone is delineated on the plots in Figure 4 by two dashed lines that represent the acceleration pulse duration times of 10 ms and 30 ms. For pulse durations less than 10 ms, the tissue strain is predominantly dependent on the peak angular velocity, and for pulse durations greater than 30 ms, the tissue strain is predominantly dependent on the peak angular acceleration. In between 10 ms and 30 ms, the tissue strain is dependent on both peak angular velocity and peak angular acceleration.

To identify the regions of the brain that experience the largest strains, the normalized strain results are plotted for the coronal rotation case in Figure 5 for varying applied magnitudes of angular acceleration and angular velocity. From this figure, it is evident that the spatial distribution of strain does not change significantly when the peak angular acceleration and angular velocity is varied. Although the magnitude of the strain is dependent on the applied loading condition (as shown in Figure 4), the location of the peak strains within the brain is relatively consistent for all applied loading conditions as long as the rotation direction remains the same. For the three rotation directions analyzed in this study, the largest strains occur at the periphery of the cerebral cortex, primarily concentrated within the gyri and sulci. For the coronal rotation case, elevated strains are also found within the frontal lobes, temporal lobes, and the boundary between the pons and medulla. The results for the sagittal and axial loading cases are shown in the Supplementary Materials. For the axial rotation case, the strains are concentrated fairly uniformly along the outer boundary of the cortex. For the sagittal rotation case, the largest strains are found within the gyri of the parietal lobe and upper portion of the occipital lobe as well as within the brainstem and upper portion of the cerebellum near the tentorium cerebellum.

To study the effect of the choice of strain measure on the cumulative strain response, cumulative critical strain maps were generated using two different definitions of strain: maximum axonal strain (MAS) and maximum principal strain (MPS). MAS accounts for the anisotropic nature of the white matter whereas MPS does not. The brain regions that exceed a strain threshold of 15% are highlighted in red. In Figure 6a, a 15% MPS threshold is applied to all brain tissue elements. In contrast in Figure 6b, the 15% MPS threshold is applied to the gray matter, and a 15% MAS threshold is applied to the white matter (i.e., the white matter regions are highlighted in red only if the strain component in the direction of fiber alignment exceeds 15%). In both sets of results, the brain tissue material model remains the same. At low inertial loads, the strains are concentrated in the outer cortex, but as the inertial loads increase, the subcortical regions of the brain also begin to exceed the strain threshold. Comparing Figures 6a and b, a smaller percentage of the brain tissue is highlighted in red in Figure 6b due to the use of the anisotropic strain measure that takes directionality into account. This is also evident in the area fraction contour plots shown in Figure 6c and Figure 6d, where a smaller area fraction of the brain is shown to exceed the strain threshold when an anisotropic measure of strain is applied. Figure 6c shows the results when a MPS threshold is applied to all brain tissue elements whereas in Figure 6d, the MPS threshold is applied to the gray matter and the MAS threshold is applied to the white matter. The area fraction is on average 26.8% lower when an anisotropic measure of strain is used, with a maximum percent difference in area fraction of 45.4%. These differences highlight the importance of choosing an appropriate definition of strain when evaluating cumulative damage within the brain.

The shape of the contour lines in the area fraction plots is similar to that of the peak strain contour lines in Figure 4. The contour lines are vertical when the acceleration magnitude is large, and they are horizontal when the acceleration magnitude is small. Therefore, the peak angular velocity has a larger effect on the area fraction when the acceleration is large. This can also be observed in Figure 6a. The area fraction of the brain that is highlighted in red is relatively unchanged as you move to the right along the bottom row of cumulative strain maps

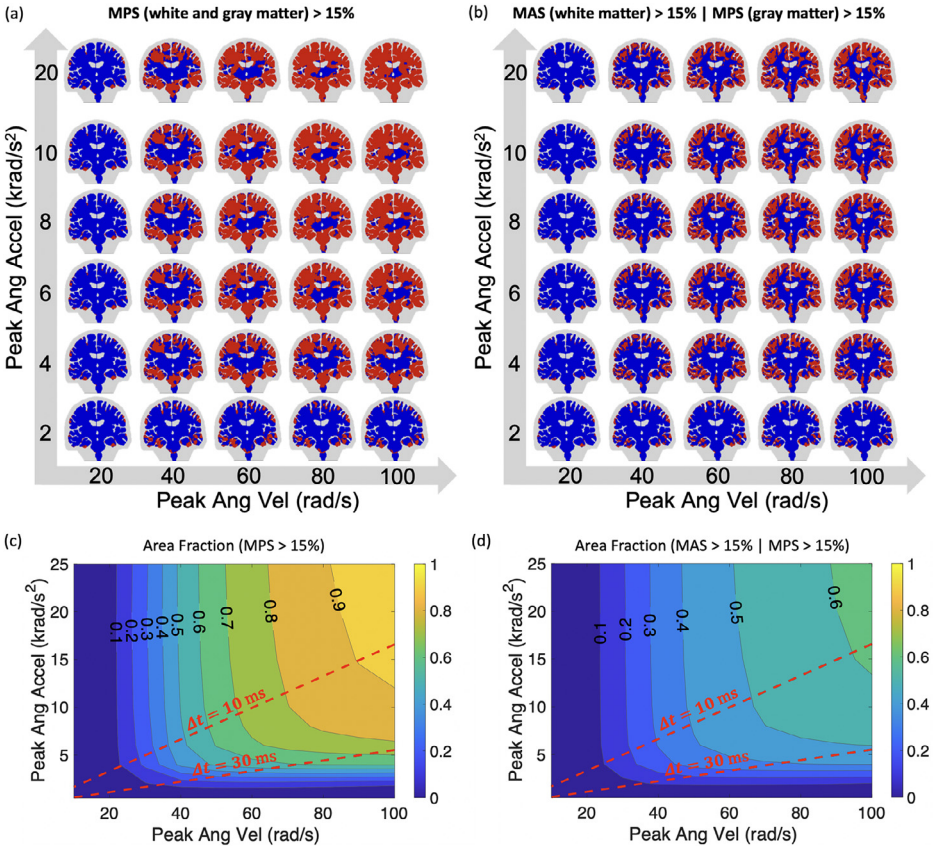

Fig. 6. Cumulative strain maps (top) are shown for the coronal rotation case, where the brain tissue elements that exceed a 15% strain threshold are highlighted in red for different applied magnitudes of angular acceleration and angular velocity. The area fraction of the brain highlighted in red is also depicted in the contour plots (bottom). Results are shown for two different measures of strain. In (a,c), the maximum principal strain (MPS) threshold is applied to all brain tissue elements. In (b,d), the maximum axonal strain (MAS) threshold is applied to the white matter elements, and the MPS threshold is applied to the gray matter elements.

where the angular acceleration is 2 krad/s^2; however, a greater change in the area fraction is observed as you move to the right along the top row of strain maps where the angular acceleration is 20 krad/s^2. This trend is observed for both cumulative strain maps. This analysis has also been repeated using a strain threshold value of 25% (see Supplementary Materials). When a larger strain threshold value is applied, the total area fraction of the brain that exceeds the threshold value decreases; however, the general trends (e.g., shape of the contours) remain the same.

3.2. Effect of Head Kinematics on Peak Strain Rates

The peak strain rates were also assessed to study the effect of the kinematic parameters on the tissue strain rate. The 3-D surface and contour plots of the peak strain rates for each rotation direction are shown in Figure 7. All results are shown for the low angular jerk case. In the surface plots, the peak strain rate values are plotted along the vertical axis, and the peak angular acceleration and peak angular velocity magnitudes are plotted along the horizontal axes. Similar to the peak strain results, axial rotations produced the largest strain rates for a given kinematic input. Coronal rotations produced the second highest strain rates, followed by sagittal rotations. The maximum percent difference in the peak strain rates between the axial and coronal models was 35.0%, and the maximum percent difference between the coronal and sagittal models was 19.6%. Since the sagittal plane does not have geometric symmetry about the axis of rotation, we also assessed the effect of rotation direction within the sagittal plane. The maximum percent difference in peak strain rate between positive and negative rotation directions was found to be 9.4% for the sagittal plane (see Supplementary Materials for corresponding strain rate contour plots).

When comparing the shape of the strain rate contours in Figure 7 with the shape of the strain contours in Figure 4, there are some noticeable differences and similarities. There is greater curvature in the strain rate contours when the acceleration magnitude is large whereas the strain contours remained relatively vertical. However, similar to the strain contours, the strain rate contours are relatively horizontal when the acceleration magnitudes are small. A transition in the curvature of the strain rate contours occurs when the acceleration pulse duration time is about 10 ms as shown by the dashed line in Figure 7. Therefore, unlike the peak strain, which is predominantly dependent on the angular acceleration for pulse durations less than 10 ms, the peak strain rate is dependent on both the angular velocity and angular acceleration at shorter pulse durations. At pulse durations greater than 10 ms, the tissue strain rate is predominantly dependent on the angular acceleration.

Plots of the normalized MPSR are shown in Figure 8 for coronal rotation. Similar to the MPS distribution, the distribution of MPSR is relatively consistent for all kinematic loading conditions, with the largest strain rates occurring at the periphery of the outer cortex. Large strain rates are also localized along the falx cerebri, which is a stiff membrane located between the cerebral hemispheres. Comparing the MPS distribution in Figure 5 with the MPSR distribution in Figure 8, there is a high degree of overlap in the regions of the brain that experience the largest strain and strain rates, indicating that the regions of the brain that experience the largest strains also tend to experience the largest strain rates. Similar trends are also found for the axial and sagittal rotation cases, which are included in the Supplementary Materials.

The cumulative strain rate maps and area fraction contour plots are shown in Figure 9 for the coronal rotation case. A strain rate threshold value of 40 s^{-1} was used to generate these plots. In Figure 9a, gray and white matter elements that exceed a MPSR threshold of 40 s^{-1} are highlighted in red. In Figure 9b, gray matter elements that exceed a MPSR threshold of 40 s^{-1} and white matter elements that exceed a MASR threshold of 40 s^{-1} are highlighted in red. As the inertial loads are increased, a larger proportion of the brain exceeds the strain rate thresholds. Comparing the cumulative strain map in Figure 6 with the cumulative strain rate map in Figure 9 for the same applied kinematic condition, the area fraction of the brain that is highlighted in red is quite different between the two figures. The area fraction is smaller when a strain rate threshold of 40 s^{-1} is applied as compared to a

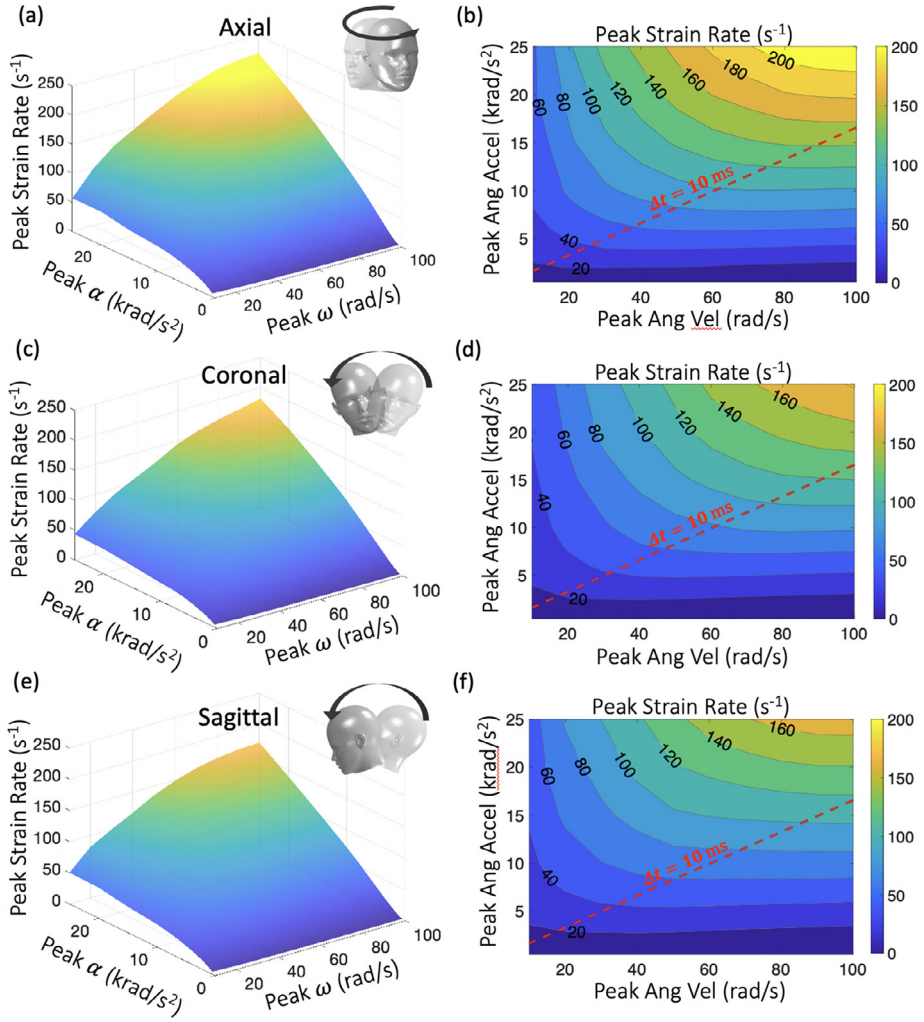

Fig. 7. The effect of angular velocity ω and angular acceleration α on the peak tissue strain rate is shown. In the left column, the peak tissue strain rate is plotted along the vertical axis in the 3-D surface plots, and the results are shown for the (a) axial, (c) coronal, and (e) sagittal models. In the right column, contour plots of the peak tissue strain rates are shown for the (b) axial, (d) coronal, and (f) sagittal models.

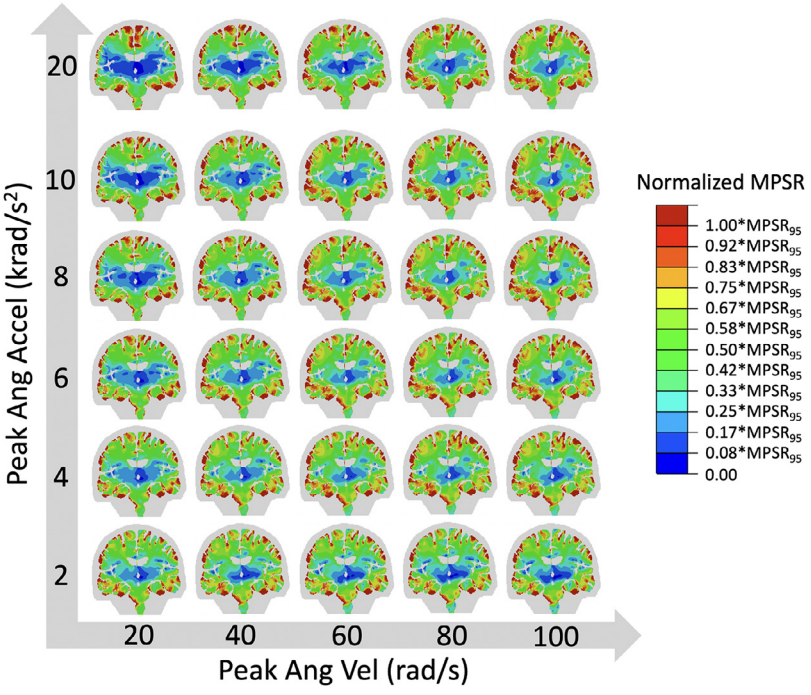

Fig. 8. The normalized maximum principal strain rate (MPSR) distribution within the coronal plane is plotted for different applied magnitudes of angular acceleration and angular velocity. The strain rate distribution represents the peak MPSR from each brain tissue element over the course of a simulation. The magnitude of the strain rates for each kinematic condition have been normalized by the 95th percentile strain rate value ($MPSR_{95}$) for that kinematic condition, which can be obtained from Figure 7.

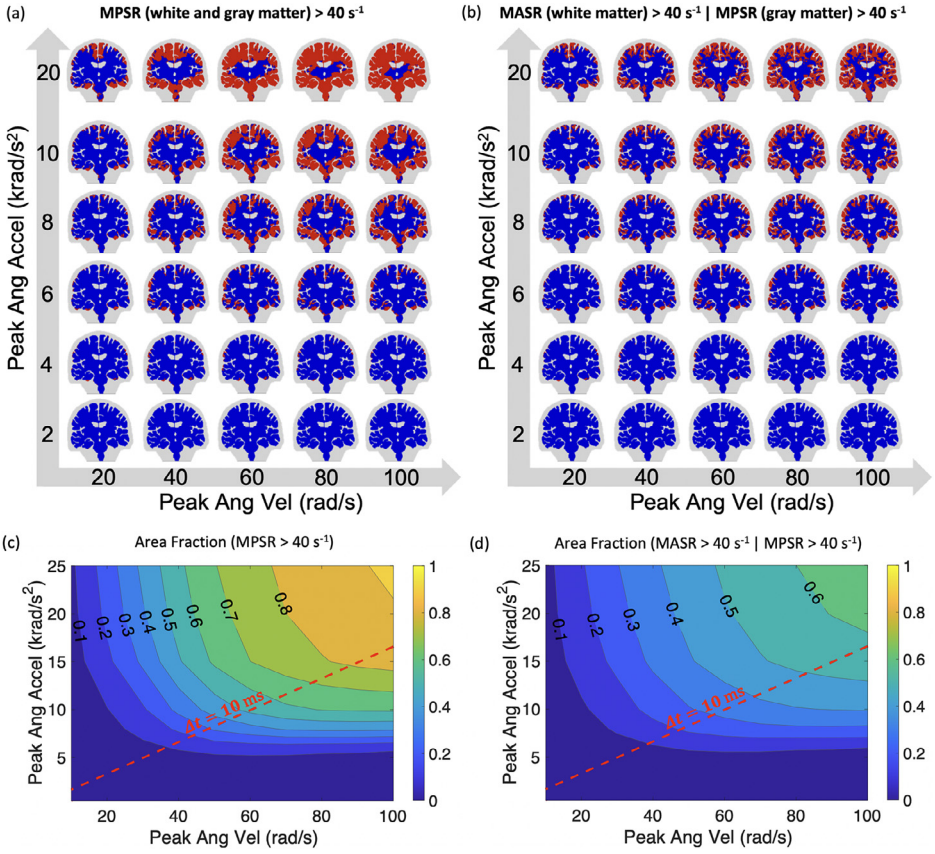

Fig. 9. Cumulative strain maps (top) are shown for the coronal rotation case, where the brain tissue elements that exceed a 40 s^{-1} strain rate threshold are highlighted in red for different applied magnitudes of angular acceleration and angular velocity. The area fraction of the brain highlighted in red is also depicted in the contour plots (bottom). Results are shown for two different measures of strain rate. In (a,c), the maximum principal strain rate (MPSR) threshold is applied to all brain tissue elements. In (b,d), the maximum axonal strain rate (MASR) threshold is applied to the white matter elements, and the MPSR threshold is applied to the gray matter elements.

strain threshold of 15%. This result is highly dependent on the chosen threshold values. If a smaller strain rate or larger strain threshold value was applied, there would be greater similarity in the total area fraction and in the locations of the brain that are highlighted in red for a given kinematic condition. Given that there isn't a consensus on the appropriate strain and strain rate thresholds to use when evaluating axonal injury, it is unclear which parameter is the dominant factor in the development of cumulative brain damage. Results generated using other strain and strain rate thresholds are included in the Supplementary Materials.

The shape of the area fraction contours in Figures 9c and 9d is similar to the peak strain rate contours in Figure 7. Therefore, the area fraction of the brain tissue that exceeds the strain rate threshold is dependent on both the angular velocity and angular acceleration at shorter pulse durations, and it is predominantly dependent on the angular acceleration at larger pulse durations. The choice of the definition of strain rate (MPSR vs. MASR) is also shown to have an effect on the strain rate results. There is a decrease in the area fraction of the brain that exceeds the strain rate threshold when an anisotropic definition of strain rate (MASR) is applied. This is due to the additional constraint that takes directionality into account. The area fraction is on average 24.0% lower when an anisotropic measure of strain rate is used, with a maximum percent difference in the area fraction of 44.7%.

3.3. Effect of Angular Jerk on Brain Deformation

To investigate the effect of angular jerk (i.e., the rate of change of the angular acceleration) on the tissue strains and strain rates, the parametric study was conducted for both low and high angular jerk acceleration loading profiles. The high jerk loading profiles had a peak angular jerk that was 50 times larger than the low jerk profiles. The results of the jerk analysis are shown in Figure 10 for the axial rotation case. Contour plots of the peak strain, peak strain rate, pulse duration, area fraction of the brain above a 15% MPS threshold, and area fraction of the brain above a 40 s^{-1} MPSR threshold are shown for both the low angular jerk case (blue curves) and the high angular jerk case (red curves). A comparison of the pulse durations for the low and high jerk case are also shown in Figure 10e. For a given kinematic input, a high angular jerk magnitude will correspond to a shorter pulse duration.

Comparing the red and blue curves in the plots, it is evident that angular jerk has a larger effect on the tissue strain rates than on the tissue strains. The average percent difference in the peak strain rate between the low and high jerk case is 20.1% whereas the average percent difference in the peak strain is only 4.0%. In Figure 10a, the strain contours are almost identical (0.2% average percent difference) for kinematic conditions that correspond to a small pulse duration (i.e., < 10 ms for the low jerk case and < 6 ms for the high jerk case). For larger pulse durations, the average percent difference is 7.2%. When considering the area fraction of the brain above a 15% MPS threshold, the average percent difference between the low and high jerk results is 12.4% (Figure 10c). When using a 40 s^{-1} MPSR threshold, the average percent difference is 25.7% (Figure 10d). Based on these results, it can be concluded that angular jerk has a larger effect on the peak strain rate developed in the brain. The effect of angular jerk on the peak strains is minimal, especially for impacts that occur over a short time duration.

4. Discussion

4.1. Effect of Angular Acceleration and Angular Velocity

The results of this study emphasize the importance of accounting for the effects of both angular acceleration and angular velocity on brain deformation. Both of these kinematic measures are shown to influence the tissue strains and strain rates that develop within the brain. Furthermore, the relative contribution of angular acceleration and angular velocity on the brain deformation response is shown to be dependent on loading duration as illustrated in Figure 11. When the acceleration pulse duration is short (< 10 ms for the low angular jerk case), the tis-

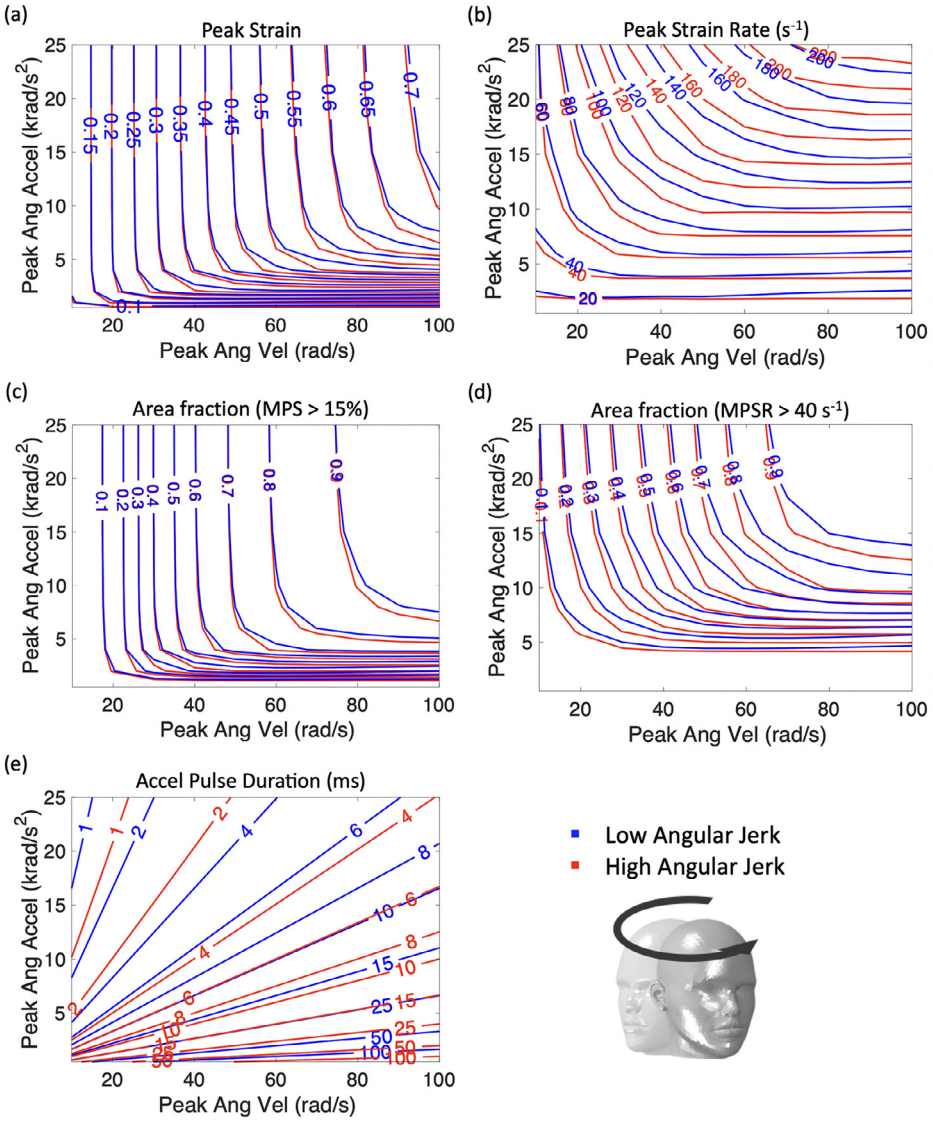

Fig. 10. The effect of angular jerk on the brain tissue response. Contour plots of the (a) peak strain, (b) peak strain rate, (c) area fraction of the brain above 15% MPS, (d) area fraction of the brain above 40 s^{-1} MPSR, and (e) acceleration pulse duration are shown for rotation about the axial plane. The blue curves represent the low angular jerk case, and the red curves represent the high angular jerk case.

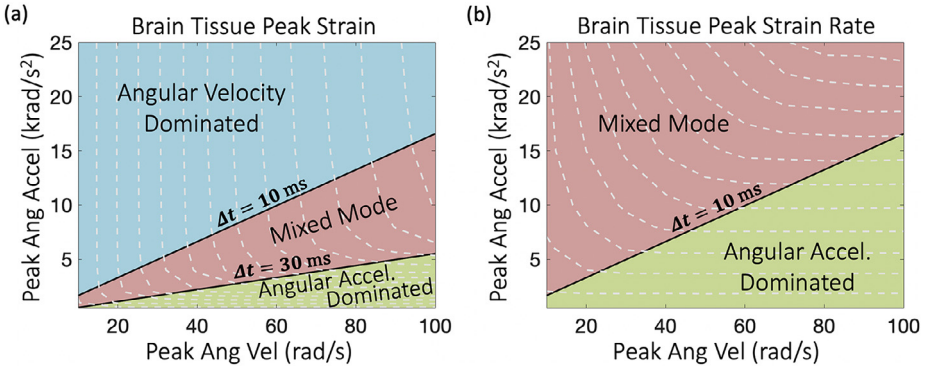

Fig. 11. These phase diagrams show the regimes where the angular velocity dominates, angular acceleration dominates, or where both angular acceleration and angular velocity have an influence (i.e., mixed mode) on the (a) brain tissue peak strains and (b) brain tissue peak strain rates. The acceleration pulse duration times (Δt) shown are for the low angular jerk case.

sue strain is predominantly dependent on the peak angular velocity. The tissue strain rate, on the other hand, is dependent on both the peak angular velocity and peak angular acceleration at these shorter pulse durations. The peak angular acceleration plays a larger role in both the tissue strains and strain rates when the pulse duration is long (> 30 ms for the low angular jerk case). For intermediate pulse durations (10 ms < Δt < 30 ms), the tissue strain rate is primarily dependent on the peak angular acceleration whereas the tissue strain is affected by both the peak angular velocity and the peak angular acceleration. These results help explain prior studies that have found stronger correlations between angular velocity or angular acceleration with tissue strain. For example, Hernandez and Camarillo found in very low frequency voluntary head motions, the maximum principal strain was more sensitive to changes in angular acceleration [21]. This observation is supported by our results. Since the time duration of voluntary head motions is long (> 100 ms), we would expect a stronger influence of angular acceleration on the peak strains. In contrast, Yoganandan et. al. found that angular velocity correlated better with strain magnitude [49]. The kinematic conditions

that were applied in their study fall within a regime where the peak angular velocity would have a larger impact on strain.

The results of our study are also consistent with the results of several recent parametric studies. Gabler et al. performed a parametric study using two different 3-D FE head models and found that the maximum brain deformation depended primarily on angular velocity for short duration pulses and on angular acceleration for long duration pulses [31], which is consistent with our results. It was also observed that the brain deformation depended on both the velocity and acceleration magnitudes for pulse durations close to the natural period of the brain-skull system, which was represented by a single-degree-of-freedom mechanical model. The effect of angular kinematics on tissue strain rate was not investigated in their study. Another parametric study by Hajiaghamemar et al. found a similar relationship between the angular velocity, angular acceleration, and maximum tissue strain using a porcine FE head model [3]. They found that the deformation responses were dominated by the peak angular velocity for short duration loadings and by angular acceleration for long duration loadings. Furthermore, their study investigated the effect of angular kinematics on the strain rate response and found that strain rate correlated more with the peak angular acceleration than peak angular velocity. This observation is also consistent with our findings where the peak strain rate was shown to be primarily dependent on the peak angular acceleration over a larger range of pulse durations when compared to the peak strain. Although the Hajiaghamemar study was based on angular motions of a porcine FE head model, which has a quite different skull geometry from the human head, similar trends were found between the angular acceleration, angular velocity, and brain deformation.

4.2. Effect of Angular Jerk

Few studies have systematically investigated the effect of angular jerk on the brain deformation response while controlling for the angular acceleration and angular velocity magnitudes. A recent FE parametric study by Saboori and Walker found that jerk had a negligible effect on the maximum principal strain when an input acceleration profile was applied directly to the center of the forehead [50]. The maximum jerk magnitude in their study was 2.5 times larger than the smallest jerk magnitude. In our study, we assessed the peak strains and peak strain rates resulting from angular motions where the maximum angular jerk magnitude was 50 times larger than the minimum jerk magnitude. When we controlled for the magnitude of the peak angular acceleration and peak angular velocity, the angular jerk was found to have minimal effect on the peak strains, especially for short pulse durations. When the pulse duration exceeded 10 ms, the effect of angular jerk on the peak strains was a bit more pronounced. Overall, we found that the angular jerk had a much larger effect on the peak strain rates than on the peak strains, with an average percent difference of about 20% in the peak strain rate magnitude between the low and high angular jerk case.

Angular jerk magnitudes of real-world head impacts are most likely closer in magnitude to the low angular jerk case used in this study than the high angular jerk case. Peak angular jerk magnitudes are not widely reported in head impact studies, but a study by Bartsch et al. [51] reported the peak angular jerk of the head resulting from an oblique hook punch from an amateur boxer to be 1.42×10^6 rad/s^3. Applying the peak angular velocity and peak angular acceleration measured in their study to the idealized acceleration profiles used in our study, it would correspond to a peak angular jerk of 1.25×10^6 rad/s^3 for the low angular jerk case and a peak angular jerk of 6.3×10^7 rad/s^3 for the high angular jerk case. Therefore, the angular jerk magnitude measured in their study is much closer in magnitude to the low angular jerk magnitude used in our study. Although the angular jerk is shown to have an effect on the peak strain rates, more information about the peak angular jerk of real-world head impacts is needed to assess the importance of reducing angular jerk to minimize the peak strain rates that develop within the brain.

4.3. Effect of Rotation Direction

When comparing rotations about the axial, coronal, and sagittal planes, axial rotations produced the largest tissue strains and strain rates, followed by coronal rotations and then sagittal rotations. Axial rotations also resulted in a larger area fraction of the brain exceeding the strain and strain rate thresholds used in our study. When comparing the rotation directions that produced the largest (i.e., axial) and smallest (i.e., sagittal) deformation, the maximum percent difference in the peak strain and peak strain rate was 49.3% and 52.7%, respectively. These results emphasize the importance of taking rotation direction into account when evaluating the brain deformation response. This directional dependence has also been observed in other studies. In measurements of brain motion of human post-mortem subjects, axial rotations were shown to produce larger brain deformations compared to sagittal and coronal rotations [52]. Several finite element modeling studies have also found larger predicted cumulative damage as a result of axial rotations compared to sagittal and coronal rotations [31,53,54].

4.4. Choice of Strain and Strain Rate Measure to Evaluate Cumulative Damage

The results of this study highlight the importance of choosing an appropriate definition of strain and strain rate when evaluating the cumulative damage that develops within the brain. The use an anisotropic measure of strain was found to have a small effect on the overall 95th percentile peak values (< 5% difference), but it had a much larger effect on the cumulative area fraction. The cumulative area fraction of the brain that exceeded a strain threshold of 15% or a strain rate threshold of 40 s^{-1} was on average around 25% smaller (and at a maximum 45% smaller) when an anisotropic measure of strain or strain rate was used, such as MAS or MASR, as compared to the case when MPS or MPSR was applied. This reduction in area fraction is due to the additional constraint that takes directionality into account. Therefore, the choice of strain measure can have a significant impact on the predicted cumulative damage and locations of injury. The cumulative strain damage measure (CSDM) is widely used as a measure of injury in finite element head modeling studies, which is based on the volume fraction of the brain that exceeds a given maximum principal strain threshold [25]. We would expect to see a reduction in the total volume fraction of the brain exceeding the strain threshold if an anisotropic measure of strain was applied instead of the maximum principal strain. Several recent studies have suggested that axonal strain or fiber-oriented strain may be a better predictor of axonal injury [15,22,24,55]; therefore, it will be important to further investigate the relationship between anisotropic strain measures, cumulative damage, and injury severity.

4.5. Locations of Peak Strains and Strain Rates

Identifying the locations of peak strains and strain rates in the brain is important to determine which regions of the brain are more vulnerable to injury. Our results show that the largest strains and strain rates tend to be concentrated within the gyri and depths of the sulci of the outer cortex of the brain, primarily within the cerebral gray matter. These locations correlate well with regions that have been shown to have increased accumulation of hyperphosphorylated tau in cases of chronic traumatic encephalopathy (CTE), which is a neurodegenerative disease caused by repetitive traumatic brain injuries [56]. In addition to the cerebral cortex, elevated strains and strain rates were also found in the cerebellum and brainstem under sagittal rotations. As the inertial loads were increased, subcortical regions of the brain also began to experience large strains. These results are consistent with prior studies. In a computational study by Lu et al. of dynamic head rotation, strains were shown to highest in the cerebral gray matter, followed by the white matter, and then the deep gray matter substructures, such as the thalamus [57]. Large strains have been shown to occur within the brainstem

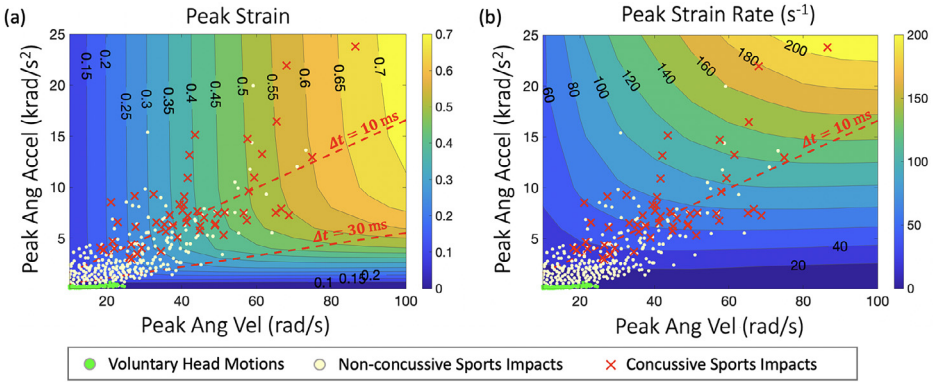

Fig. 12. Head impact kinematic data from published studies [21,34,42,65–68] are overlaid on the peak tissue strain and strain rate contour plots for axial rotation. The green circular markers represent voluntary head motions, the light yellow circular markers represent non-concussive sports impacts, and the red x's represent impacts that resulted in diagnosed concussion.

[54,58,59] and cerebellum [59] under sagittal rotations in both finite element modeling and tagged magnetic resonance studies. The corpus callosum, which is another region of the brain that has been identified as being susceptible to injury [34,60,61], did not undergo large strains at low inertial loads in our study; however, strains in the corpus callosum exceeded a MPS threshold of 15% under coronal rotation as the inertial loads were increased.

Interestingly, although the magnitude of strains was dependent on the applied inertial loads, the spatial distribution of the strains did not change significantly for different applied angular accelerations and velocities as long as the rotation direction remained the same. This suggests that the path taken by the stress waves in the brain from an applied inertial load is not dependent on the shape of the wave. The shape of the wave, however, is a direct result of the applied loading condition and has an effect on the deformation magnitude. Given these results, if the normalized spatial distribution of strain is known for a single kinematic condition, the strain distribution can be estimated for other kinematic conditions by scaling the magnitude of the strains as long as the direction of rotation remains the same. An estimate of this scaling factor for angular accelerations about the coronal, sagittal, and axial planes can be obtained from Equation S1 in the Supplementary Materials. This equation was empirically derived from Figures 4 and 7 and provides an estimate of the peak strains and peak strain rates. These strain distribution results have important implications, suggesting that the brain deformation response for a large range of kinematic conditions can be estimated from a subset of finite element modeling results. There are currently efforts to estimate brain strains using such an approach [62–64].

4.6. Comparison with Real-world Head Impact Data

While most kinematic measures of TBI focus on evaluating injury risk [1], an advantage of connecting kinematics to injury through strain and strain rate is that the measure is still valid when new strain and strain rate injury thresholds become available, which is still an ongoing area of research. To illustrate how our results relate to real-world head impact data, we have plotted head impact kinematic data from published studies on the axial rotation peak tissue strain and strain rate contour plots in Figure 12. The impact data includes voluntary head motion data from Hernandez et al. [21], and concussive and non-concussive sports head impact data from a number of studies [34,42,65–68]. It should be noted that the head impact data is plotted based on resultant measures of peak angular velocity and peak angular acceleration since the axial component of these kinematic measurements was not reported in all studies. From these plots, we can observe that non-injurious impacts tend to occur over longer durations of time as compared to injurious impacts. Furthermore, the peak strains and peak strain rates also tend to be larger for injurious impacts. There isn't, however, a clear distinction between non-concussive and concussive impacts in terms of defining a strain and strain rate threshold for injury. This could be due to a number of factors, including undetected concussive injuries, effects of repetitive loading, errors in kinematic measurements, directional effects, and intra-individual variability. It is also possible there may not be a simple strain and strain rate threshold for injury and a more complex relationship may exist between strain, strain rate, and injury risk. Part of this challenge is that the diagnosis of concussion itself is neurosymptomatic [69]. That is, it relies on downstream effects of brain injury to manifest. Yet, more recent work has shown that brain injury without concussive signs, often referred to as subconcussive, can be an equally significant source of brain injury [70]. A further exploration of the role of each of these factors is needed to have a clearer picture of the relationship between head kinematics and injury risk.

4.7. Limitations

In this study, we assessed the tissue strains and strain rates that resulted from an idealized angular acceleration loading profile. Fully understanding the effect of angular acceleration alone on the brain deformation response is an important step towards elucidating the relationship between angular kinematics and injury risk; however, in future work, the effect of deceleration on the tissue strain and strain rate response should also be characterized. Real-world head impacts are complex and include both angular acceleration and deceleration. The time duration of the deceleration response can influence the peak strains and peak strain rates that develop within the brain. For example, prior studies have shown that when angular accelerations and decelerations are applied over a short duration, strain magnitudes in the brain are reduced [53]. Given that it takes about 10 ms for a shear wave to traverse to the center of the brain [41], pulse durations shorter than this time period will result in unloading of the tissue before the strains are fully developed. In contrast, larger tissue strains will result if angular decelerations are applied over a longer duration of time or if there is a long time interval separating the acceleration and deceleration pulse [49,53].

Another limitation of this study is that the FE analysis was performed separately for each rotation direction. In real-world head impacts, head motions may involve multiple components of angular acceleration, and it is important to consider the effect of directional coupling on the tissue strains and strain rates. Several studies have investigated the effect of rotation direction, including off-axis rotational directions, on the tissue strains and have found that the peak strain and cumulative strain are dependent on the components of rotation, suggesting a coupling behavior [52–54,71]. However, other studies have suggested that the coupling behavior has a minimal impact on the peak strains that develop within the brain. In the development of the DAMAGE injury metric, Gabler et al. found that the influence of off-axis motions was relatively small, and a coupled model only had a small improvement over the uncoupled model [32]. It will be important in future work to systematically study the effect of directional coupling on the brain deformation response.

The results of this study are based on the output of an FE head model, and therefore, the accuracy of the brain deformation prediction is de-

pendent on the accuracy of the FE model. Our parametric study was performed using 2-D finite element head models along the axial, coronal, and sagittal planes. Although these FE models were well validated against existing low and high rate head impact experimental datasets, these datasets do not cover the full range of possible head impact scenarios. We are also limited to validating the high strain rate behavior using cadaveric data, which may not be representative of the mechanical response of living tissue [72]. These limitations are not unique to our study, and the validation of finite element head models remains a challenge. Another limitation of the FE model is that the brain geometry was based on a single subject. Differences in brain geometry between individuals have been shown to affect the strain distribution that develops in the brain [73]. Brain tissue properties may also change with age or from repeated head impact exposures [72,74,75]. In future work, a sensitivity analysis will be conducted to study the effect of brain geometry and tissue properties on the brain deformation results.

We also chose to use 2-D FE head models instead of a 3-D model to conduct this study. An advantage of 2-D simulations are that they are less computationally expensive than 3-D simulations, which allows greater anatomical detail to be incorporated into these models without a significant increase in computational cost. The 2-D head models used in our study had a higher spatial resolution and included more anatomical detail (e.g., inclusion of gyri and sulci, anisotropy, etc.) compared to the 3-D head models commonly used to develop kinematic-based injury metrics. One limitation of 2-D models is that they cannot capture the out-of-plane tissue response. Despite this limitation, they provide useful information about the in-plane deformations. Recent tagged magnetic resonance imaging studies of rotational head motions about the axial and sagittal planes have shown that the largest strain components occur within the plane of rotation [59]. Furthermore, the largest deformations were shown to occur in slices with the most brain tissue present, such as near the mid-sagittal plane and in axial planes passing through the lateral ventricles. Since our models were based on brain slices near the center of the brain and contain the ventricles, the maximum tissue strains within these slices should be representative of the maximum tissue strains in the brain. In future work, the results of the 2-D FE head models will be further verified by comparing the brain deformation predictions of the 2-D model with a 3-D model for a subset of impact conditions.

5. Conclusion

In this study, we have conducted a large scale parametric FE analysis to provide further insight into the relationship between angular head motion and brain deformation. The effect of angular acceleration, angular velocity, and angular jerk on the peak tissue strains and strain rates was analyzed. The results of the parametric study show that both angular acceleration and angular velocity can have a significant effect on the brain deformation response, with the relative contribution of each being dependent on the acceleration pulse duration. Angular jerk, on the other hand, had a minimal effect on the peak tissue strains when the peak angular acceleration and angular velocity were held constant, but it did have a larger effect on the peak strain rates. While the peak strains and strain rates were affected by the applied kinematic condition, this study revealed that the spatial distribution of strain did not change significantly as long as the rotation direction remained the same, which has important implications when developing methods to rapidly estimate the brain deformation response. With an improved understanding of the relationship between angular kinematics and brain deformation, we can begin to develop new strategies for mitigating and preventing traumatic brain injury.

Declaration of Competing Interest

The authors declare no competing interests.

Acknowlgedgments

This work used the Extreme Science and Engineering Discovery Environment (XSEDE), which is supported by National Science Foundation grant number ACI-1548562. Specifically, it used the Bridges system, which is supported by NSF award number ACI-1445606, at the Pittsburgh Supercomputing Center (PSC). The authors acknowledge the Panther program for facilitating fruitful discussions and collaborations, and acknowledge Nomin Khishigsuren for help in compiling literature data for Figure 12. CF, ALF, YW, and HK acknowledge funding from the ONR Panther program (Dr. Timothy Bentley), grant N00014-17-1-2644 and N00014-21-1-2044.

Supplementary Material

Supplementary material associated with this article can be found, in the online version, at 10.1016/j.brain.2021.100024

References

[1] F.A. Fernandes, R.J.A. de Sousa, Head injury predictors in sports trauma–a state-of-the-art review, Proc. Inst. Mech. Eng. Pt. H J. Eng. Med. 229 (8) (2015) 592–608.
[2] S. Kleiven, Why most traumatic brain injuries are not caused by linear acceleration but skull fractures are, Front. Bioeng. Biotechnol. 1 (2013) 15.
[3] M. Hajiaghamemar, M. Seidi, S.S. Margulies, Head rotational kinematics, tissue deformations, and their relationships to the acute traumatic axonal injury, J. Biomech. Eng. 142 (3) (2020).
[4] D. Sahoo, C. Deck, R. Willinger, Brain injury tolerance limit based on computation of axonal strain, Accid. Anal. Prev. 92 (2016) 53–70.
[5] D.H. Smith, D.F. Meaney, Axonal damage in traumatic brain injury, Neuroscientist 6 (6) (2000) 483–495.
[6] M.D. Tang-Schomer, V.E. Johnson, P.W. Baas, W. Stewart, D.H. Smith, Partial interruption of axonal transport due to microtubule breakage accounts for the formation of periodic varicosities after traumatic axonal injury, Exp. Neurol. 233 (1) (2012) 364–372.
[7] E. Bar-Kochba, M.T. Scimone, J.B. Estrada, C. Franck, Strain and rate-dependent neuronal injury in a 3D in vitro compression model of traumatic brain injury, Sci. Rep. 6 (1) (2016) 1–11.
[8] A.C. Bain, D.F. Meaney, Tissue-level thresholds for axonal damage in an experimental model of central nervous system white matter injury, J. Biomech. Eng. 122 (6) (2000) 615–622.
[9] L. Zhang, K.H. Yang, A.I. King, A proposed injury threshold for mild traumatic brain injury, J. Biomech. Eng. 126 (2) (2004) 226–236.
[10] B.S. Elkin, B. Morrison, Region-specific tolerance criteria for the living brain, SAE Tech. Pap. (2007).
[11] E.G. Takhounts, M.J. Craig, K. Moorhouse, J. McFadden, V. Hasija, Development of brain injury criteria (BrIC), SAE Tech. Pap. (2013).
[12] S. Kleiven, Predictors for traumatic brain injuries evaluated through accident reconstructions, SAE Tech. Pap. (2007).
[13] H. Ahmadzadeh, D.H. Smith, V.B. Shenoy, Viscoelasticity of tau proteins leads to strain rate-dependent breaking of microtubules during axonal stretch injury: predictions from a mathematical model, Biophys. J. 106 (5) (2014) 1123–1133.
[14] H. Nakadate, E. Kurtoglu, H. Furukawa, S. Oikawa, S. Aomura, A. Kakuta, Y. Matsui, Strain-rate dependency of axonal tolerance for uniaxial stretching, SAE Tech. Pap. (2017).
[15] S. Sullivan, S.A. Eucker, D. Gabrieli, C. Bradfield, B. Coats, M.R. Maltese, J. Lee, C. Smith, S.S. Margulies, White matter tract-oriented deformation predicts traumatic axonal brain injury and reveals rotational direction-specific vulnerabilities, Biomech. Model. Mechanobiol. 14 (4) (2015) 877–896.
[16] D.K. Cullen, C.M. Simon, M.C. LaPlaca, Strain rate-dependent induction of reactive astrogliosis and cell death in three-dimensional neuronal–astrocytic co-cultures, Brain Res. 1158 (2007) 103–115.
[17] M. Hajiaghamemar, S.S. Margulies, Multi-scale white matter tract embedded brain finite element model predicts the location of traumatic diffuse axonal injury, J. Neurotrauma (2020).
[18] S.S. Margulies, L.E. Thibault, A proposed tolerance criterion for diffuse axonal injury in man, J. Biomech. 25 (8) (1992) 917–923.
[19] A. Post, M. Kendall, D. Koncan, J. Cournoyer, T.B. Hoshizaki, M.D. Gilchrist, S. Brien, M.D. Cusimano, S. Marshall, Characterization of persistent concussive syndrome using injury reconstruction and finite element modelling, J. Mech. Behav. Biomed. Mater. 41 (2015) 325–335.
[20] J.G. Beckwith, W. Zhao, S. Ji, A.G. Ajamil, R.P. Bolander, J.J. Chu, T.W. McAllister, J.J. Crisco, S.M. Duma, S. Rowson, et al., Estimated brain tissue response following impacts associated with and without diagnosed concussion, Ann. Biomed. Eng. 46 (6) (2018) 819–830.
[21] F. Hernandez, D.B. Camarillo, Voluntary head rotational velocity and implications for brain injury risk metrics, J. Neurotrauma 36 (7) (2019) 1125–1135.
[22] S. Ji, W. Zhao, J.C. Ford, J.G. Beckwith, R.P. Bolander, R.M. Greenwald, L.A. Flashman, K.D. Paulsen, T.W. McAllister, Group-wise evaluation and comparison of white

matter fiber strain and maximum principal strain in sports-related concussion, J. Neurotrauma 32 (7) (2015) 441–454.
[23] W. Zhao, Y. Cai, Z. Li, S. Ji, Injury prediction and vulnerability assessment using strain and susceptibility measures of the deep white matter, Biomech. Model. Mechanobiol. 16 (5) (2017) 1709–1727.
[24] C. Giordano, S. Zappalà, S. Kleiven, Anisotropic finite element models for brain injury prediction: the sensitivity of axonal strain to white matter tract inter-subject variability, Biomech. Model. Mechanobiol. 16 (4) (2017) 1269–1293.
[25] E.G. Takhounts, R.H. Eppinger, J.Q. Campbell, R.E. Tannous, E.D. Power, L.S. Shook, On the development of the SIMon finite element head model, Technical Report, SAE Tech. Pap., 2003.
[26] A. Post, E. Hashim, T.B. Hoshizaki, M.D. Gilchrist, M.D. Cusimano, A preliminary examination of the relationship between biomechanical measures and structural changes in the brain, Trauma (2020).
[27] L.E. Miller, J.E. Urban, E.M. Davenport, A.K. Powers, C.T. Whitlow, J.A. Maldjian, J.D. Stitzel, Brain strain: computational model-based metrics for head impact exposure and injury correlation, Ann. Biomed. Eng. (2020) 1–14.
[28] J.S. Giudice, W. Zeng, T. Wu, A. Alshareef, D.F. Shedd, M.B. Panzer, An analytical review of the numerical methods used for finite element modeling of traumatic brain injury, Ann. Biomed. Eng. 47 (9) (2019) 1855–1872.
[29] A. Madhukar, M. Ostoja-Starzewski, Finite element methods in human head impact simulations: a review, Ann. Biomed. Eng. 47 (9) (2019) 1832–1854.
[30] P. Dixit, G. Liu, A review on recent development of finite element models for head injury simulations, Arch. Comput. Methods Eng. 24 (4) (2017) 979–1031.
[31] L.F. Gabler, H. Joodaki, J.R. Crandall, M.B. Panzer, Development of a single-degree-of-freedom mechanical model for predicting strain-based brain injury responses, J. Biomech. Eng. 140 (3) (2018).
[32] L.F. Gabler, J.R. Crandall, M.B. Panzer, Development of a second-order system for rapid estimation of maximum brain strain, Ann. Biomed. Eng. 47 (9) (2019) 1971–1981.
[33] L.F. Gabler, J.R. Crandall, M.B. Panzer, Development of a metric for predicting brain strain responses using head kinematics, Ann. Biomed. Eng. 46 (7) (2018) 972–985.
[34] K. Laksari, M. Fanton, L.C. Wu, T.H. Nguyen, M. Kurt, C. Giordano, E. Kelly, E. O'Keeffe, E. Wallace, C. Doherty, et al., Multi-directional dynamic model for traumatic brain injury detection, J. Neurotrauma 37 (7) (2020) 982–993.
[35] R.M. Wright, A. Post, B. Hoshizaki, K.T. Ramesh, A multiscale computational approach to estimating axonal damage under inertial loading of the head, J. Neurotrauma 30 (2) (2013) 102–118.
[36] A.M. Nahum, R. Smith, C.C. Ward, Intracranial pressure dynamics during head impact, SAE Tech. Pap. (1977).
[37] A.A. Sabet, E. Christoforou, B. Zatlin, G.M. Genin, P.V. Bayly, Deformation of the human brain induced by mild angular head acceleration, J. Biomech. 41 (2) (2008) 307–315.
[38] C. Thunert, CORAplus Release 4.0.4 User's Manual, 2017.
[39] W.N. Hardy, M.J. Mason, C.D. Foster, C.S. Shah, J.M. Kopacz, K.H. Yang, A.I. King, J. Bishop, M. Bey, W. Anderst, et al., A study of the response of the human cadaver head to impact, Stapp Car Crash J. 51 (2007) 17.
[40] Z. Zhou, X. Li, S. Kleiven, C.S. Shah, W.N. Hardy, A reanalysis of experimental brain strain data: Implication for finite element head model validation, Stapp Car Crash J. (2018) 293–318.
[41] Y. Chen, M. Ostoja-Starzewski, MRI-based finite element modeling of head trauma: spherically focusing shear waves, Acta Mech. 213 (1-2) (2010) 155–167.
[42] E. O'Keeffe, E. Kelly, Y. Liu, C. Giordano, E. Wallace, M. Hynes, S. Tiernan, A. Meagher, C. Greene, S. Hughes, et al., Dynamic blood–brain barrier regulation in mild traumatic brain injury, J. Neurotrauma 37 (2) (2020) 347–356.
[43] R.M. Wright, K. Ramesh, An axonal strain injury criterion for traumatic brain injury, Biomech. Model. Mechanobiol. 11 (1-2) (2012) 245–260.
[44] R.W. Carlsen, N.P. Daphalapurkar, The importance of structural anisotropy in computational models of traumatic brain injury, Front. Neurol. 6 (2015) 28.
[45] S. Chatelin, C. Deck, F. Renard, S. Kremer, C. Heinrich, J.-P. Armspach, R. Willinger, Computation of axonal elongation in head trauma finite element simulation, J. Mech. Behav. Biomed. Mater. 4 (8) (2011) 1905–1919.
[46] R.H. Kraft, P.J. Mckee, A.M. Dagro, S.T. Grafton, Combining the finite element method with structural connectome-based analysis for modeling neurotrauma: Connectome neurotrauma mechanics, PLoS Comput. Biol. 8 (8) (2012) e1002619.
[47] D. Sahoo, C. Deck, R. Willinger, Axonal strain as brain injury predictor based on real-world head trauma simulations, in: Proceedings of the IRCOBI Conference, Lyon, France IRC-15-30, 2015.
[48] T. Wu, J. Antona-Makoshi, A. Alshareef, J.S. Giudice, M.B. Panzer, Investigation of cross-species scaling methods for traumatic brain injury using finite element analysis, J. Neurotrauma 37 (2) (2020) 410–422.
[49] N. Yoganandan, J. Li, J. Zhang, F.A. Pintar, T.A. Gennarelli, Influence of angular acceleration–deceleration pulse shapes on regional brain strains, J. Biomech. 41 (10) (2008) 2253–2262.
[50] P. Saboori, G. Walker, Brain injury and impact characteristics, Ann. Biomed. Eng. 47 (9) (2019) 1982–1992.
[51] A. Bartsch, E. Benzel, V. Miele, D. Morr, V. Prakash, Impact 'fingerprints' and preliminary implications for an 'intelligent mouthguard' head impact dosimeter, Sports Eng. 15 (2) (2012) 93–109.
[52] A. Alshareef, J.S. Giudice, J. Forman, D.F. Shedd, K.A. Reynier, T. Wu, S. Sochor, M.R. Sochor, R.S. Salzar, M.B. Panzer, Biomechanics of the human brain during dynamic rotation of the head, J. Neurotrauma (2020).
[53] K. Bian, H. Mao, Mechanisms and variances of rotation-induced brain injury: a parametric investigation between head kinematics and brain strain, Biomech. Model. Mechanobiol. (2020) 1–19.
[54] A.A. Weaver, K.A. Danelson, J.D. Stitzel, Modeling brain injury response for rotational velocities of varying directions and magnitudes, Ann. Biomed. Eng. 40 (9) (2012) 2005–2018.
[55] M. Hajiaghamemar, T. Wu, M.B. Panzer, S.S. Margulies, Embedded axonal fiber tracts improve finite element model predictions of traumatic brain injury, Biomech. Model. Mechanobiol. (2019) 1–22.
[56] A.C. McKee, T.D. Stein, C.J. Nowinski, R.A. Stern, D.H. Daneshvar, V.E. Alvarez, H.-S. Lee, G. Hall, S.M. Wojtowicz, C.M. Baugh, et al., The spectrum of disease in chronic traumatic encephalopathy, Brain 136 (1) (2013) 43–64.
[57] Y.-C. Lu, N.P. Daphalapurkar, A. Knutsen, J. Glaister, D. Pham, J. Butman, J.L. Prince, P. Bayly, K. Ramesh, A 3D computational head model under dynamic head rotation and head extension validated using live human brain data, including the falx and the tentorium, Ann. Biomed. Eng. 47 (9) (2019) 1923–1940.
[58] B.S. Elkin, L.F. Gabler, M.B. Panzer, G.P. Siegmund, Brain tissue strains vary with head impact location: A possible explanation for increased concussion risk in struck versus striking football players, Clin. Biomech. 64 (2019) 49–57.
[59] A.K. Knutsen, A.D. Gomez, M. Gangolli, W.-T. Wang, D. Chan, Y.-C. Lu, E. Christoforou, J.L. Prince, P.V. Bayly, J.A. Butman, et al., In vivo estimates of axonal stretch and 3D brain deformation during mild head impact, Brain Multiphys. (2020) 100015.
[60] F. Hernandez, C. Giordano, M. Goubran, S. Parivash, G. Grant, M. Zeineh, D. Camarillo, Lateral impacts correlate with falx cerebri displacement and corpus callosum trauma in sports-related concussions, Biomech. Model. Mechanobiol. 18 (3) (2019) 631–649.
[61] C. Giordano, S. Kleiven, Evaluation of axonal strain as a predictor for mild traumatic brain injuries using finite element modeling, SAE Tech. Pap. (2014).
[62] S. Ji, W. Zhao, A pre-computed brain response atlas for instantaneous strain estimation in contact sports, Ann. Biomed. Eng. 43 (8) (2015) 1877–1895.
[63] K. Ghazi, S. Wu, W. Zhao, S. Ji, Instantaneous whole-brain strain estimation in dynamic head impact, J. Neurotrauma (2020).
[64] V.B. Shim, S. Holdsworth, A.A. Champagne, N.S. Coverdale, D.J. Cook, T.-R. Lee, A.D. Wang, S. Li, J.W. Fernandez, Rapid prediction of brain injury pattern in mTBI by combining FE analysis with a machine-learning based approach, IEEE Access 8 (2020) 179457–179465.
[65] D.A. Patton, The Biomechanical Determinants of Sports-Related Concussion: Finite Element Simulations of Unhelmeted Head Impacts to Evaluate Kinematic and Tissue Level Predictors of Injury and Investigate the Design Implications for Soft-Shell Headgear, University of New South Wales, 2014 Ph.D. thesis.
[66] L.C. Wu, C. Kuo, J. Loza, M. Kurt, K. Laksari, L.Z. Yanez, D. Senif, S.C. Anderson, L.E. Miller, J.E. Urban, et al., Detection of American football head impacts using biomechanical features and support vector machine classification, Sci. Rep. 8 (1) (2017) 1–14.
[67] F. Hernandez, L.C. Wu, M.C. Yip, K. Laksari, A.R. Hoffman, J.R. Lopez, G.A. Grant, S. Kleiven, D.B. Camarillo, Six degree-of-freedom measurements of human mild traumatic brain injury, Ann. Biomed. Eng. 43 (8) (2015) 1918–1934.
[68] E.J. Sanchez, L.F. Gabler, A.B. Good, J.R. Funk, J.R. Crandall, M.B. Panzer, A reanalysis of football impact reconstructions for head kinematics and finite element modeling, Clin. Biomech. 64 (2019) 82–89.
[69] S.P. Broglio, K.M. Guskiewicz, J. Norwig, If you're not measuring, you're guessing: the advent of objective concussion assessments, J. Athl. Train. 52 (3) (2017) 160–166.
[70] S.M. Gysland, J.P. Mihalik, J.K. Register-Mihalik, S.C. Trulock, E.W. Shields, K.M. Guskiewicz, The relationship between subconcussive impacts and concussion history on clinical measures of neurologic function in collegiate football players, Ann. Biomed. Eng. 40 (1) (2012) 14–22.
[71] K. Taylor, T.B. Hoshizaki, A. Post, M.D. Gilchrist, The relationship between directional components of dynamic response and maximum principal strain for impacts to an american football helmet, Proc. Inst. Mech. Eng. P J. Sport. Eng. Technol. 234 (3) (2020) 193–204.
[72] S. Budday, T.C. Ovaert, G.A. Holzapfel, P. Steinmann, E. Kuhl, Fifty shades of brain: a review on the mechanical testing and modeling of brain tissue, Arch. Comput. Methods Eng. (2019) 1–44.
[73] J.S. Giudice, A. Alshareef, T. Wu, C.A. Gancayco, K.A. Reynier, N.J. Tustison, T.J. Druzgal, M.B. Panzer, An image registration-based morphing technique for generating subject-specific brain finite element models, Ann. Biomed. Eng. 48 (10) (2020) 2412–2424.
[74] I. Sack, K.-J. Streitberger, D. Krefting, F. Paul, J. Braun, The influence of physiological aging and atrophy on brain viscoelastic properties in humans, PloS One 6 (9) (2011) e23451.
[75] A.J. Romano, W.G. Szymczak, An overview of mixed-model inversion and its application to the study of traumatic brain injury, J. Acoust. Soc. Am. 148 (4) (2020) 2595.